TITLE:

Effect of second-phase particles on the properties of W-based materials under high-heat loading

AUTHOR(S):

Tan, Xiao–Yue; Li, Ping; Luo, Lai–Ma; Xu, Qiu; Tokunaga, Kazutoshi; Zan, Xiang; Wu, Yu–Cheng

CITATION:

Tan, Xiao–Yue ...[et al]. Effect of second-phase particles on the properties of W-based materials under high-heat loading. Nuclear Materials and Energy 2016, 9: 399-404

ISSUE DATE:

2016-12

URL:

http://hdl.handle.net/2433/218609

RIGHT:

© 2016 The Authors. Published by Elsevier Ltd. This is an open access article under the CC BY-NC-ND license (http://creativecommons.org/licenses/by-nc-nd/4.0/).

京都大学学術情報リポジトリ
KURENAI 紅
Kyoto University Research Information Repository

京都大学 KYOTO UNIVERSITY
A Self-archived copy in
Kyoto University Research Information Repository
https://repository.kulib.kyoto-u.ac.jp
京都大学学術情報リポジトリ KURENAI 紅 Kyoto University Research Information Repository

Nuclear Materials and Energy 9 (2016) 399–404

Contents lists available at ScienceDirect

Nuclear Materials and Energy

journal homepage: www.elsevier.com/locate/nme

Effect of second-phase particles on the properties of W-based materials under high-heat loading

Xiao–Yue Tan[a], Ping Li[a,d], Lai–Ma Luo[a,d,*], Qiu Xu[b], Kazutoshi Tokunaga[c], Xiang Zan[a,d], Yu–Cheng Wu[a,d,*]

[a] School of Materials Science and Engineering, Hefei University of Technology, Hefei 230009, China
[b] Research Reactor Institute, Kyoto University, Osaka-fu 590-0494, Japan
[c] Research Institute for Applied Mechanics, Kyushu University, Kasuga, Fukuoka 816-8580, Japan
[d] National–Local Joint Engineering Research Centre of Nonferrous Metals and Processing Technology, Hefei 230009, China

ARTICLE INFO

Article history:
Available online 3 August 2016

Keywords:
Tungsten
ITER
Plasma-facing materials
Thermal shock

ABSTRACT

W, W-TaC, and W-TiC materials were subjected to heat–load tests in an electron beam facility (10 keV, 8 kW) at 100 pulses. After heat loading, severe cracks and plastic deformation were detected on the surface of pure W materials. However, plastic deformation was the primary change on the surfaces of W-TaC and W-TiC alloys. This phenomenon was due to the second-phase (TaC and TiC) particles dispersed in the W matrix, which strengthened the grain boundaries and prevented crack formation and propagation. In addition, the microhardness of W and W-TiC obviously decreased, whereas that of W-TaC did not change considerably before and after heat loading.

© 2016 The Authors. Published by Elsevier Ltd.
This is an open access article under the CC BY-NC-ND license
(http://creativecommons.org/licenses/by-nc-nd/4.0/).

1. Introduction

Plasma-facing materials (PFMs) in thermonuclear reactors (e.g., ITER and DEMO) will be subjected to a harsh operational environment [1]. These materials have to bear high particle fluxes, such as hydrogen, helium, and neutron irradiation, caused by the interaction with burning fusion plasma. PFMs are also expected to withstand steady-state heat loads and transient events, such as plasma disruptions, edge-localized modes (ELMs), and vertical displacement events [2]. Therefore, resistance to particle irradiation and thermal load is essential for this application.

Tungsten (W) is a promising candidate as PFM because of its high melting point of ~3410 °C, high thermal conductivity of ~173 $W\,m^{-1}\,k^{-1}$ at room temperature (RT), low tritium retention, and low sputtering yield in radiation environment [3]. However, materials may exhibit brittle behavior, such as low-temperature brittleness, high-temperature or recrystallization brittleness, and radiation-induced increase of brittleness and hardness, which are due to high ductile-to-brittle transition temperature (DBTT), low recrystallization temperature, and induced defects, respectively [4]. Several failure events were previously observed in W PFMs, with considerably unacceptable short lifetime [5,6]. Crack formation of W materials is a major concern induced by thermal stress because of brittleness below the DBTT [7]. An increase in crack depth may be related to the recrystallization-induced increase of the DBTT of W materials, resulting in reduced crack resistance [8]. In addition, particle irradiation leads to a series of embrittlement concerns [9,10]. In the present study, several second-phase particles, such as TiC, TaC, and La_2O_3 [11], dispersed in the W matrix can effectively resolve the mentioned brittleness issues. Numerous grain boundaries can be obtained because the second-phase particles induce grain refinement, and they could act as sink to capture radiation-induced defects, thereby improving radiation resistance [12]. W or W alloys with ultrafine grain size are very important for decreasing the DBTT [13]. Furthermore, second-phase particles can inhibit recrystallization because of their improved high-temperature strength and creep resistance by hindering the sliding of grain boundary and stabilizing the microstructure at higher temperature [14].

This study simulated the heat load tolerance of the obtained W materials by using an electron beam irradiation device [15]. DBTT and low recrystallization temperature are the main factors of failures under heat load conditions. TaC and TiC nanoparticles, which act as second-phase particles, were used to improve the W matrix [16,17]. The second-phase nanoparticles dispersed in the grain interior and the grain boundaries could decrease the DBTT [18]. This

* Corresponding author: Fax: +86 551 62901012.
E-mail addresses: luolaima@126.com (L. Luo), ycwu@hfut.edu.cn (Y. Wu).

http://dx.doi.org/10.1016/j.nme.2016.07.009
2352-1791/© 2016 The Authors. Published by Elsevier Ltd. This is an open access article under the CC BY-NC-ND license (http://creativecommons.org/licenses/by-nc-nd/4.0/).

京都大学 KYOTO UNIVERSITY
A Self-archived copy in
Kyoto University Research Information Repository
https://repository.kulib.kyoto-u.ac.jp
京都大学学術情報リポジトリ KURENAI 紅 Kyoto University Research Information Repository

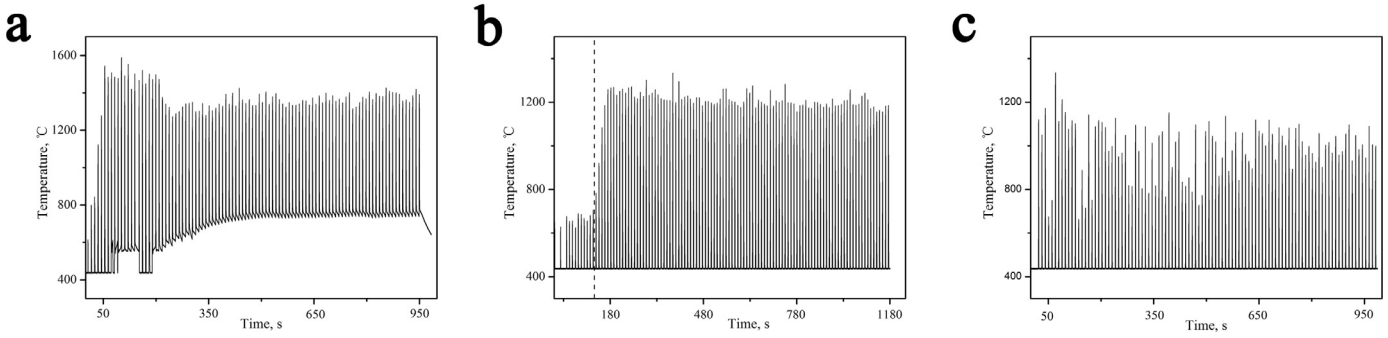

Fig. 1. Time evolution of the surface temperature of the samplesin the repeated heat loading experiments of (a) pure W, (b) W-TaC and (c) W-TiC, respectively.

dispersed structure could strengthen the grain boundaries, thereby hindering crack formation and propagation [16].

2. Experimental

The W, W-TaC, and W-TiC materials were prepared in our laboratory [16,17]. TaC and TiC were added at 1% mass fraction. Nano-sized W, W-TaC, and W-TiC powders were fabricated using a wet chemical method. The obtained powders were sintered by spark plasma technique. A cylindrical specimen, with a diameter of 6 mm and thickness of ~2 mm, was cut from the sintered bodies by using wire electric discharge mchining. Subsequently, the thermal diffusivity and the thermal shock behavior were discussed. The specimen was grinded and polished to obtain a mirror-quality surface prior to the thermal shock test. Thermal shock test was employed to simulate ELM-like events to induce damage behavior by using an electron beam facility. All polished specimens were placed on a Cu block, cooled with water, and subjected to high heat load by using an electron beam irradiation test simulator of the Research Institute for Applied Mechanics, Kyushu University [15]. The specimens were heated with an electron beam (10 keV, 8 kW, beam diameter of ~1 mm) at RT. The heat was applied mode with a loading heat of 2 s, the total cycle duration of 9.5 s and a total of 100 pulses. Surface temperature was measured by a two-color pyrometers. Changes in the surface morphology after the heat load were observed by field emission scanning electron microscopy (FESEM). The specimens were etched using an etchant solution (50 vol. % H_2O_2 + 50 vol. % $NH_3{\cdot}H_2O$) to determine the position of the change in morphology at the grain boundary or in the grain interior. Vickers microhardness of the heated specimens was measured using a MH-3 L microhardness tester, with a load of 200 gf (1.96 N) held for 15 s.

3. Results and discussion

3.1. Heat loading test

The changes in surface temperature of the specimens in the electron beam test as measured using the two-color pyrometers are presented in Fig. 1. The two-color pyrometers could only be used at temperatures above 450 °C. Fig. 1a shows the surface temperature of W versus pulse time. Initially, the beam-on surface temperature reached ~1540 °C, and decreased to below 450 °C during the rest time. The beam-on surface temperature of every pulse shows the tendency to decrease to ~1330 °C until the last pulse, and the beam-off surface temperature at every rest time shows the tendency to increase to ~740 °C. Changes in the surface temperatures of the W-1TaC and W-1TiC material versus pulse time are shown in Fig. 1b and c, respectively. The beam-on surface temperature of W-1TaC remained constant at ~1200 °C, whereas W-1TiC displayed a fluctuating beam-on surface temperature of ~1060 °C. During the rest time of each pulse, the surface temperature of W-1TaC and W-1TiC decreased to below 450 °C.

Some differences are found in the beam-on surface temperature among the W, W-1TaC, and W-1TiC samples under similar experimental parameters. This result is due to the different electronic absorption coefficients (EACs) of the W-based materials. Higher EAC indicates higher amount of electron beam energy that could be delivered to the sample, resulting in higher surface temperature. Pure W exhibited the highest EAC, and thus the highest surface temperature, whereas W-1TiC had the lowest EAC and lowest surface temperature. The beam-on surface temperature should relate to the amount of the absorbed electrons. In general, for electron beam interaction with pure substance, the pure substance with higher atomic number yield a higher amount of backscattered electrons and therefore result in lower electron absorption. For these W alloys (W-TiC, W-TaC), the content of the doped second phase only 1 wt. %. Therefore, the effect of the different composition induced different EAC was very lower. The second phase result grain refinement i.e. many areas in the alloys have been replaced by grain boundaries. The atoms arrangement disordered in these grain boundaries. For the same substance, the regions of the grain interior and grain boundary are with the same atomic number. However, the incident electrons should be more easily diffracted in grain boundaries than the case in grain interior. In contrary, the incident electrons should be lesser absorbed in grain boundaries than the case in grain interior. For the reason, pure W present higher EAC than W alloys. In our opinion, the grain boundaries induced the lower EAC act as the primary role. Therefore, pure W presents higher EAC than W alloys.

3.2. Microstructure

Base specimens before heat loading were tested at RT, i.e., below the DBTT [19]. Figs. 2, 3, and 4 show the FESEM images of the loaded surface of W, W-TaC, and W-TiC, respectively. Fig. 2a shows the FESEM image of the surface of W after 100 pulses of repeated heat loading. Test conditions are shown in Fig. 1a. During the first several pulses, the surface temperature of W was very high, yielding steep temperature and stress gradients. These characteristics induced the formation of a main arbitrary crack network within the loaded area (Fig. 2a). Fig. 2b shows a high-magnification image of the cracked area. The main cracks were occurred along the grain boundaries, which imply that the grain boundaries were the weakest part of the materials. At the following pulses, the low surface temperature of pure W was ~740 °C (higher than the DBTT), which could be attributed to the formed cracks that hindered thermal conduction. Thus, W shows plastic deformation under the applied thermal stress conditions without any brittle behavior. Fig. 2c (viewed from the black square frame area in Fig. 2a) shows surface modifications of protruding parts, small cracks, or some obvious fissures in the grain boundary. The surface modifications could be

京都大学 KYOTO UNIVERSITY
A Self-archived copy in
Kyoto University Research Information Repository
https://repository.kulib.kyoto-u.ac.jp
京都大学学術情報リポジトリ KURENAI 紅 Kyoto University Research Information Repository

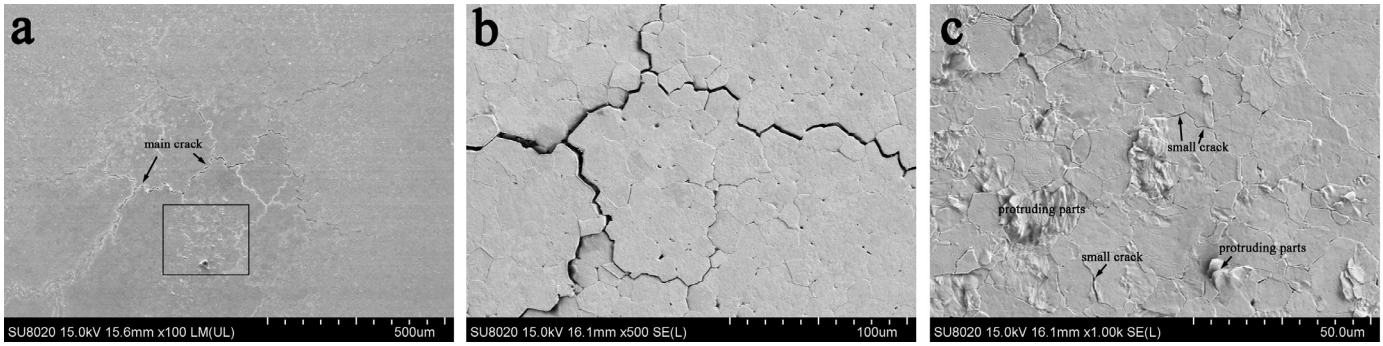

Fig. 2. (a) Low-magnification and (b) (c) high-magnification FESEM image of the surface of pure W after heat loading test.

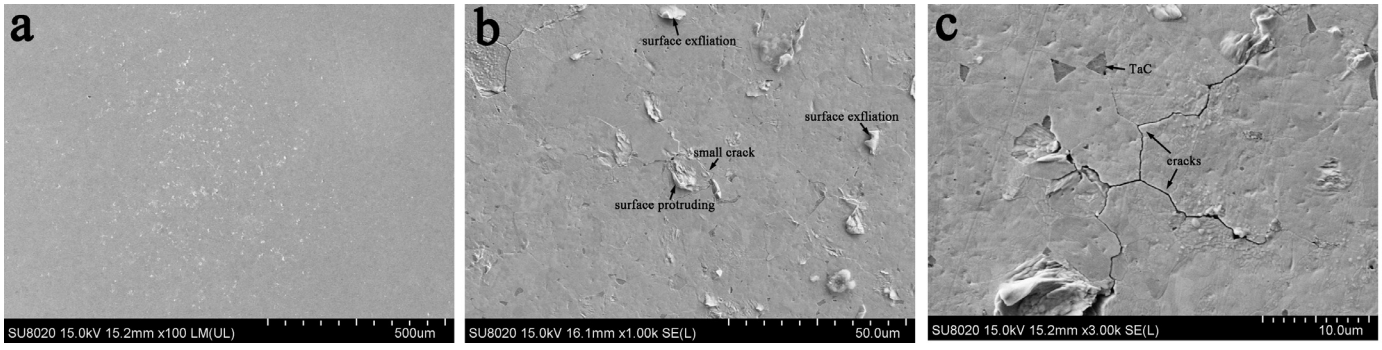

Fig. 3. (a) Low-magnification and (b) (c) high-magnification FESEM image of the surface of W-TaC alloy after heat loading test.

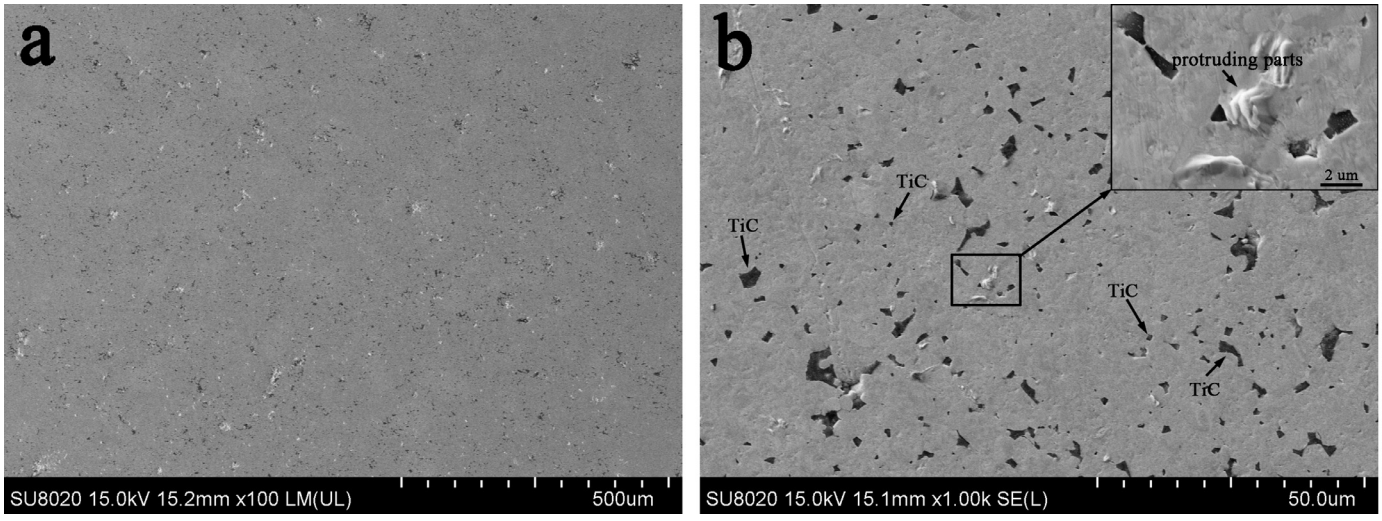

Fig. 4. (a) Low-magnification and (b) high-magnification FESEM image of the surface of W-TiC alloy after heat loading test.

attributed to plastic deformation and thermal fatigue loading, respectively. As shown in Fig. 2c, the protruding parts were located in the grain interior, which means that the plastic deformation occurs in the grain interior. Grain boundaries have higher density of defects than the grain interior, and thus plastic deformation is difficult.

During a pulse, the loaded surface temperature rapidly increases to high temperature, i.e., higher than the DBTT. The loaded hot surface expands and generates compressive stresses, which can cause deformation of W at high temperature if the thermal stresses exceed the yield strength [20]. The yield strength decreases with increasing temperature. After deformation, the material does not return to the original state in the following cool down phase [21]. Exfoliation and protrusion of parts are the results of irreversible plastic deformation. During the rest time between pulses, the surface temperature of the sample decreases, and the sample starts to shrink. This shrinkage induces tensile stresses at the loaded surface. Given that the base temperature is lower than the DBTT, the material exhibits brittle behavior, which indicates that stress relief is not possible and cracks can occur. The main crack results from the tensile stresses relieved the first cycles [22]. The cracks initiate at the weak grain boundaries. At the following cycles, the compressive and tensile stresses induced by the pulses repeatedly affect the grain boundary, eventually resulting in grain boundary detachment and formation of small cracks.

The surface morphology of W-1TaC after repeated heat loading of 100 pulses is shown in Fig. 3. No obvious cracks were observed at the loaded area (Fig. 3a). However, the white protruding part

京都大学 KYOTO UNIVERSITY
A Self-archived copy in
Kyoto University Research Information Repository
https://repository.kulib.kyoto-u.ac.jp
京都大学学術情報リポジトリ KURENAI 紅 Kyoto University Research Information Repository

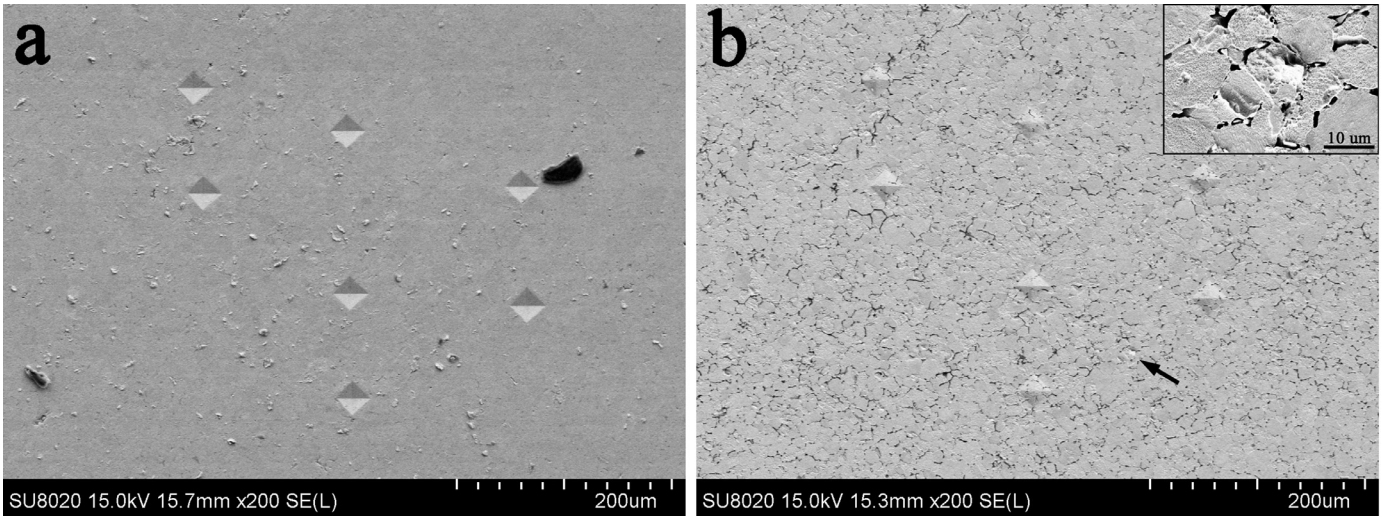

Fig. 5. FESEM image of the indentations surface of W-TaC alloy (a) after microhardness test; (b) after metallographic corrosion.

was detected in the loaded area, which could have been formed by plastic deformation. Figs. 3b and c are the high-magnification images of the regions with white protruding parts. Surface exfoliation, surface protrusion, and small crack formation were detected in Fig. 3b. The surface exfoliation and surface protrusion were the white protruding parts shown in Fig. 3a. Results of this study indicated that the cracks did not exist at the phase boundary but at the grain boundary of tungsten (such as shown in Fig. 3c), which suggests that the added TaC particles hindered heat-induced crack propagation. In addition, the phase boundaries show obviously not only owing to the different colors as the secondary electron artifact but also the existing steps between the W and TaC, which was induced from grinding and polishing during the preparation of the heat-loaded experimental sample.

Fig. 4 presents the surface morphology of W-TiC alloy after heat loading. Fewer white protruding parts were found in the W-TiC alloy compared with that on W-TaC alloy (Fig. 4a). No small crack was detected on the surface of the W-1TiC alloy as shown by the high-magnification images in Fig. 4b. The TiC particles are presented as black parts shown in Fig. 4b, and the W phase is represented by the white–gray regions. Protruding parts (indicated by the arrow in the insert image in Fig. 4b) only existed in the W-phase region, i.e., plastic deformation only occurred at the W grain. Therefore, W-TiC has an excellent performance under heat loading.

The grain boundaries in Figs. 3 and 4 are difficult to distinguish; thus, confirming where the plastic deformation occurred is difficult as well. Fig. 5a shows the surface morphology of W-1TaC alloy after microhardness test. Some white protruding parts were detected near the indentations. Fig. 5b shows the SEM image in the location of the indentations after metallographic etching. Most of the white protruding parts have disappeared, while an obvious protruding part was pointed by an arrow. The magnification image of the protruding part is presented in the inset image in Fig. 5b. The protruding part existed in the grain interior, i.e., the plastic deformation occurred in the grain interior of the W-1TaC alloy. This result agrees well with that in the pure W materials as shown in Fig. 2c. For the W-1TiC alloy, the white protruding parts were too small to be observed after metallographic etching.

Thus, doping second-phase TaC and TiC could effectively improve the resistance of heat-loaded materials, and W-TiC alloy had the best performance. Crack formation generally has a damage threshold value, i.e., thermal stress induced by heat loading should exceed the threshold value to generate crack. During the cooling down phase, cracks formed at the grain boundary because tensile stress exceeded the strength of the grain boundary. Second-phase nanoparticles were dispersed at the grain boundary and strengthened it [23]. Thus, doping TaC and TiC enhanced the strength of the grain boundary and prevented crack formation. For the same ratio of 1 wt.% of TaC and TiC, TiC presented a higher volume fraction than TaC. The higher volume of TiC with microsized dispersed particles resulted in more effectively strengthened grain boundaries and an improved resistance to crack formation compared with that of TaC. Moreover, plastic deformation would be hampered at the grain boundary during heat loading given that the second-phase particles strengthened the grain boundary; this phenomenon should be the other reason of the occurrence of plastic deformation at the grain interior. However, thermal stress induced by high thermal gradients could not be relieved by plastic deformation only. For the W-TaC alloy, the thermal fatigue induced small crack was also another method to relieve the thermal stress.

Table 1
Microhardness of the samples before and after heat loading.

Micro-hardness (Hv)	Pure W	W-1TaC	W-1TiC
Un-heat loaded	304.9	347.9	422.8
Central loaded area	233.5	337.4	358.5
Surrounding area	261.2	356.8	369.3

3.3. Microhardness

Microhardness of the samples was tested before and after loading. The diameter of the circulars samples for heat load experiments was 6 mm, and the electron beam spot was ~1 mm. Both the central loaded area (which the electron beam heated directly) and the surrounding area that experienced no direct electron beam load were affected by the effective heat at the central loaded area. The microhardness values are summarized in Table 1. From Table 1, W-TiC showed the highest microhardness, which was due to its highest volume ratio of second-phase distributed in the W matrix with microsized particles. The microhardness of pure W and W-TiC alloy considerably declined after heat loading. For pure W, this result could be primarily caused by the evident cracks as shown in Fig. 2. Fig. 6 shows the indentation of the W-TiC alloy after microhardness test. Findings showed some microcracks and microprotrusions in or near the indentation. This should be the reason for the decline of W-TiC alloy microhardness. The central

京都大学 KYOTO UNIVERSITY
A Self-archived copy in
Kyoto University Research Information Repository
https://repository.kulib.kyoto-u.ac.jp
京都大学学術情報リポジトリ KURENAI 紅 Kyoto University Research Information Repository

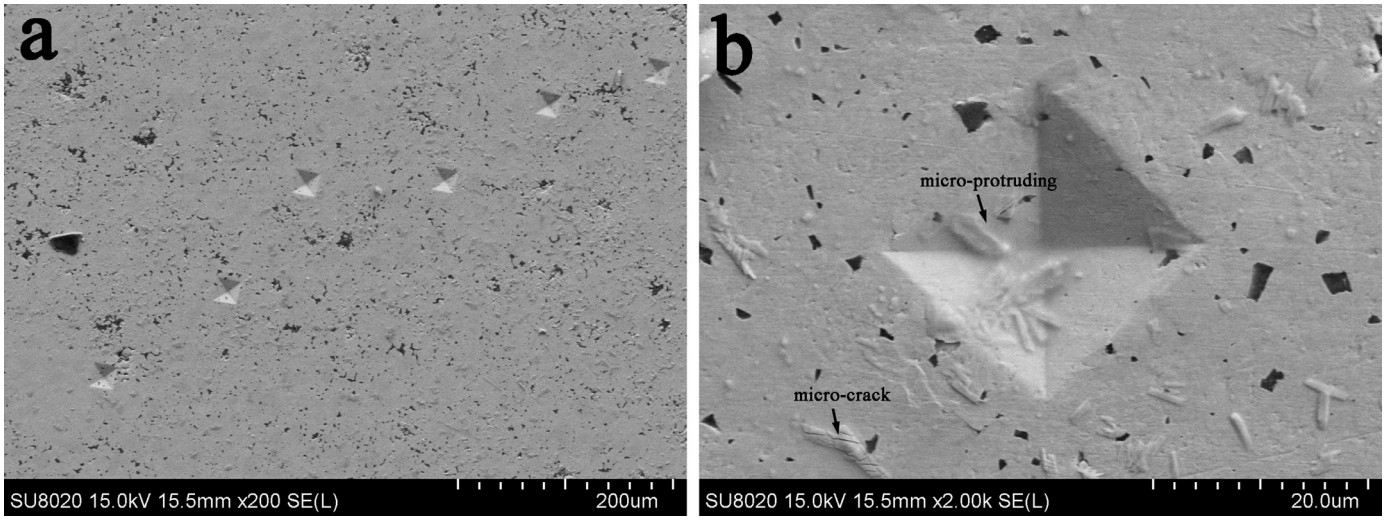

Fig. 6. FESEM image of the indentation morphology of the W-TiC alloy after microhardness test.

Table 2
The Grain size, Density, Relative density, and Thermal conductivity effective of the pure W and W alloys.

materials	Grain size (um)	Density (g/cm^3)	Relative density (%)	Thermal conductivity (W·m^{-1}K^{-1}) RT
Pure W	15	18.8	97.2	148.3
W-1TaC	12	18.6	96.5	183.8
W-1TiC	6	18.52	99.0	122.9

loaded area exhibited lower microhardness values than the surrounding area. However, the microhardness values of W-TiC at the central loaded area and at the surrounding area showed no obvious difference. The microhardness values of W-TaC alloy before and after loading varied only marginally. The microhardness at the central loaded area decreased from 347.9 MPa to 337.4 MPa, whereas that of the surrounding area slightly increased to approximately 356.8 MPa.

Microhardness is generally related to various factors, such as density, grain size, and second-phase particle dopants, which increased the density of defects to strengthen the materials. Table 2 [16,17] shows these effective factors of pure W and W alloys. The present paper proposes that thermal conductivity is closely related with the changes of microhardness under heat loading. W-TaC has excellent thermal conductivity, i.e., heat does not have a lasting effect on the surface of the materials. During the 100 pulses, the induced thermal stress (compressive and tensile stresses) did not severely affect the entire loaded area of the W-TaC alloy, except for a little area affected with slight plastic deformation and small amount of small cracks. Microhardness characterization is unable to reflect this slight effect on damages on the microstructure, which could result in obvious changes of the microhardness. The parts of the materials under the central heat-loaded area are directly exposed to the electron beam, resulting in more serious heat damage than the surrounding area. Thus, lower microhardness value was measured at the central heat-loaded area. W-TiC showed the lowest thermal conductivity, which resulted in a longer heat effect on the surface of the alloy. The FESEM images in Fig. 4 show that slight plastic deformation only could relive the limited thermal stress which induced from the heat-loading experimental. Therefore, some microstructures (microcracks or microprotrusions shown in Fig. 6) are inferred to relieve thermal stress and reduce microhardness.

4. Conclusion

W, W-TaC, and W-TiC materials were prepared in our laboratory. After heat loading using an electron beam facility (10 keV, 8 kW) at a 100 pulse cycle, severe cracks and plastic deformation were detected on the surface of the heat-loaded area on pure W. Small amount of cracks and slight plastic deformation were observed on the surface of W-TaC. Only slight plastic deformation was found in the W-TiC alloy. Some microcracks and microprotrusions observed in W-TiC alloy should be attributed to other mechanisms to relieve thermal stress. Second-phase (TaC and TiC) particles played a critical role when dispersed in the W matrix by enhancing the strength of grain boundaries and preventing crack formation and propagation. Thermal conductivity may be closely related with the changes of microhardness after heat loading. Therefore, W and W-TiC showed evident changes in microhardness. By contrast, W-TaC showed no considerable change in microhardness.

This study showed that doping of second-phase particles TaC and TiC have a positive effect in improving the resistance of heat-loaded W matrix materials. In terms of resistance to thermal shock, W-TaC and W-TiC alloys can be considered promising PFMs for fusion reactors.

Acknowledgments

This work is supported by National Magnetic Confinement Fusion Program (Grant No. 2014GB121001), National Natural Science Foundation of China (Grant No. 51474083 and 51574101), and Natural Science Foundation of Anhui Province (Grant No. 1408085QE83).

References

[1] M. Wirtz, J. Linke, G. Pintsuk, L. Singheiser, M. Zlobinski, J. Nucl. Mater. 438 (2013) S833–S836.
[2] M. Wirtz, J. Linke, G. Pintsuk, J. Rapp, G.M. Wright, J. Nucl. Mater. 420 (2012) 218–221.

京都大学 KYOTO UNIVERSITY
A Self-archived copy in
Kyoto University Research Information Repository
https://repository.kulib.kyoto-u.ac.jp
京都大学学術情報リポジトリ KURENAI 紅 Kyoto University Research Information Repository

[3] X.Y. Tan, P. Li, L.M. Luo, H.Y. Chen, X. Zan, X.Y. Zhu, G.N. Luo, Y.C. Wu, Fusion Eng. Des. 100 (2015) 571–575.
[4] X.Y. Tan, L.M. Luo, H.Y. Chen, X.Y. Zhu, X. Zan, G.N. Luo, J.L. Chen, P. Li, J.G. Cheng, D.P. Liu, Y.C. Wu. Sci. Rep. 5 12755.
[5] M. Wirtz, J. Linke, G. Pintsuk, L. Singheiser, I. Uytdenhouwen, Phys. Scr. T145 (2011) 014058.
[6] Th. Loewenhoff, A. Bürger, J. Linke, G. Pintsuk, A. Schmidt, L. Singheiser, C. Thomser, Phys. Scr. T145 (2011) 014057.
[7] T. Hirai, G. Pintsuk, J. Linke, M. Batilliot, J. Nucl. Mater. 390-391 (2009) 751–754.
[8] G. Pintsuk, A. Prokhodtseva, I. Uytdenhouwen, J. Nucl. Mater. 417 (2011) 481–486.
[9] H. Trinkaus, B.N. Singh, J. Nucl. Mater. 323 (2003) 229–242.
[10] M. Fukuda, A. Hasegawa, S. Nogami, K. Yabuuchi, J. Nucl. Mater. 1-3 (2014) 213–S218.
[11] J.L. Fan, Y. Han, P.F. Li, Z.Y. Sun, Q. Zhou, J. Nucl. Mater. 455 (2014) 717–723.
[12] X.Y. Tan, L.M. Luo, H.Y. Chen, P. Li, G.N. Luo, X. Zan, J.G. Cheng, Y.C. Wu, Powder Technol. 280 (2015) 83–88.
[13] C.C. Ge, Z.J. Zhou, S.X. Song, J. Du, Z.H. zhong, J. Nucl. Mater. 363-365 (2007) 1211–1215.
[14] M. Fukuda, A. Hasegawa, T. Tanno, S. Nogami, H. Kurishita, J. Nucl. Mater. 442 (2013) S273–S276.
[15] K. Tokunaga, K. Matsumoto, Y. Miyamoto, T. Muroga, N. Yoshida, J. Nucl. Mater. 212-215 (1994) 1323.
[16] X.Y. Tan, L.M. Luo, Z.L. Lu, G.N. Luo, X. Zan, J.G. Cheng, Y.C. Wu, Powder Technol. 269 (2015) 437–442.
[17] L.M. Luo, X.Y. Tan, H.Y. Chen, G.N. Luo, X.Y. Zhu, J.G. Cheng, Y.C. Wu, Powder Technol. 273 (2015) 8–12.
[18] G. Liu, G.J. Zhang, F. Jiang, X.D. Ding, Y.J. Sun, J. Sun, E. Ma, Nat. Mater. 12 (2013) 344–350.
[19] T. Hirai, K. Ezato, P. Majerus, Materials Transactions 46 3 (2005) 412–424.
[20] J. Linke, T. Loewenhoff, V. Massaut, G. Pintsuk, G. Ritz, M. Rodig, A. Schmidt, C. Thomser, I. Uytdenhouwen, V. Vasechko, M. Wirtz, Nucl. Fusion 51 (2011) 073017.
[21] Th. Loewenhoff, J. Linke, G. Pintsuk, C. Thomser, Fusion Eng. Des. 87 (2012) 1201–1205.
[22] M. Wirtz, J. Linke, G. Pintsuk, G. De Temmerman, G.M. Wright, J. Nucl. Mater. 443 (2013) 497–501.
[23] N. Lemahieu, J. Linke, G. Pintsuk, G.V. Oost, M. Wirtz, Z. Zhou, Phys. Scr. T159 (2014) 014035.